HHS Public Access

Author manuscript

J Affect Disord. Author manuscript; available in PMC 2023 February 15.

Published in final edited form as:

J Affect Disord. 2022 February 15; 299: 207–214. doi:10.1016/j.jad.2021.12.005.

White matter markers and predictors for subject-specific rTMS response in major depressive disorder

Lipeng Ning[1,2,3,*], **Yogesh Rathi**[1,3], **Tracy Barbour**[2,3], **Nikos Makris**[2,3], **Joan A. Camprodon**[2,3]

[1]Brigham and Women's Hospital, Boston, MA, USA

[2]Massachusetts General Hospital, Boston, MA, USA

[3]Harvard Medical School, Boston, MA, USA

Abstract

Repetitive transcranial magnetic stimulation (rTMS) has established therapeutic efficacy for major depressive disorder (MDD). While translational research has focused primarily on understanding the mechanism of action of TMS on functional activation and connectivity, the effects on structural connectivity remain largely unknown especially when rTMS is applied using subject-specific brain targets. This study aims to use novel diffusion magnetic resonance imaging (dMRI) analysis to examine microstructural changes related to rTMS treatment response using a unique cohort of 21 patients with MDD treated using rTMS with subject-specific targets. White matter dMRI microstructural measures and clinical scores were captured before and after the full course of treatment. We defined disease-relevant fiber bundles connected to different subregions of the left prefrontal cortex and analyzed changes in diffusion properties as well as correlations between the changes of dMRI measures and the changes in Hamilton Depression Rating Scale (HAMD). No significant changes were observed in tracts connected to the TMS targets. rTMS significantly increased the extra-axonal free-water volume, fractional anisotropy and decreased the radial diffusivity in anterior-medial prefrontal fiber bundles but did not lead to raw changes in lateral prefrontal tracts. That said, the microstructural changes in the lateral prefrontal white matter were significantly correlated with treatment response. Moreover, pre-rTMS dMRI measures of the dorsal anterior cingulate cortex and lateral prefrontal cortex connections are correlated with changes in HAMD scores. Microstructural changes in the anterior-medial and lateral prefrontal white matter are potentially involved in treatment response to TMS, though further investigation is needed using larger datasets.

[*]Corresponding author: Lipeng Ning, Psychiatry Neuroimaging Laboratory, 1249 Boylston St., Boston, MA 02215, Phone: +1-617-6256024, lning@bwh.harvard.edu.

6. Author Statement

LN performed the experiments and wrote the manuscript. YR revised the manuscript. TB contributed to clinical data analysis. NM conceived the experiment. JAC designed the experiment and revised the manuscript.

Declaration of Competing Interest

The authors declare they have no conflicts of interest.

Keywords

transcranial magnetic stimulation; depression; diffusion MRI; neural plasticity; predictor

1. Introduction

Repetitive transcranial magnetic stimulation (rTMS) is a safe and effective noninvasive device neuromodulation treatment for neuropsychiatric conditions, including major depressive disorder (MDD) [1, 2]. The two FDA-cleared TMS antidepressant protocols use excitatory modulation (10Hz rTMS or intermittent Theta Burst Stimulation) over the left dorsolateral prefrontal cortex (DLPFC). The stimulation target is typically selected using the “5 cm rule”, i.e., the center of the TMS coil is placed 5 cm anterior to the primary motor cortex representation of the hand. In recent years, the functional connectivity of brain networks has been utilized to improve rTMS antidepressant efficacy by defining targets in the group space or individual patients [3, 4]. While the functional connectivity related to rTMS treatment for MDD has been investigated, the underlying structural pathways related to treatment response remain unclear. Moreover, the inter-subject differences in functional brain networks and anatomical structures may impact the effect of TMS on different white-matter tracts for different subjects. Thus, understanding the changes in individualized target-specific and generic disease- relevant white-matter connections can provide useful insights to understanding the mechanism of rTMS treatment response.

The goal of this work is to examine rTMS-related microstructural changes from a cohort of 21 MDD patients who were treated with rTMS using subject-specific stimulation targets based on functional connectivity (FC) from the subgenual cortex to the DLPFC. Because of inter-subject differences in brain connectivity, these subjects had different stimulation targets across the left frontal cortex where the underlying brain regions were determined based on electric field (E-field) simulations [5]. The diverse target locations of this unique cohort of subjects provided rich information to investigate the following three problems in rTMS treatment for MDD: 1) Does rTMS lead to changes in the microstructure of white-matter fiber bundles connected to the stimulation site, despite the inter-subject differences in target locations? 2) Is rTMS treatment response related to common changes in MDD-related white-matter fiber bundles? 3) Is the treatment response related to or predicted by the microstructure of specific white-matter fiber bundles before rTMS treatment?

To investigate these problems, we have developed a novel method to investigate the microstructure of white-matter fiber bundles. Our method integrates the free-water corrected diffusion tensor model [6–8] with a multi-fiber diffusion tractography algorithm [8–11] to examine the free-water (FW) volume, free-water-corrected fractional anisotropy (FAt), radial diffusivity (RD) and axial diffusivity (AD) of fiber bundles. This method can separate isotropic fast-diffusion component in the extra axonal space and anisotropic slow-diffusion in the intra-axonal space to enhance the sensitivity and specificity of imaging measures [7, 12, 13]. The FW measure quantifies the volume fraction of relatively fast diffusing water in the extra axonal space within each voxel. Thus, the change of the FW measure after the treatment can reflect the alterations of the extracellular space which may be related to

neuroinflammation [8]. The RD, AD and FAt measures are obtained after separating the free-water component in dMRI signals which specifically quantify the microstructure of the intra axonal space. RD and AD reflect the water diffusivity in perpendicular plane and along the axonal directions, respectively. The FAt reflects the directionality of water displacement and takes value between 0 (isotropic diffusivity) and 1 (diffusivity along a straight line) to characterize the shape of the intra axonal space. Thus, the four dMRI measures can reflect the response of different tissue structures to rTMS to provide comprehensive information about the underlying mechanism. We applied these dMRI measures in the following analysis to address the three questions in above.

Microstructure changes in target-specific brain connections:

A hypothesis on the mechanism for antidepressant treatment is that rTMS can indirectly stimulate MDD-related deep-brain regions trans-synaptically via the structural pathways connecting to distal regions. To examine if rTMS changes the microstructure of the underlying white-matter fiber bundles, we extracted the dMRI tractography results between the individual stimulation targets and four deep-brain regions affected in the pathophysiology of MDD, including the SGC [3, 4, 14–16], the dorsal anterior cingulate cortex (dACC) [17–20], rostral anterior cingulate cortex (rACC) [20–23], and genu of corpus callosum (CC) [24, 25]. We compared the dMRI measures of these target- and patient-specific fiber bundles before and after rTMS to investigate the effect of rTMS. We also examined if these microstructure changes were correlated with the reduction of the Hamilton Depression Rating Scale (HAMD) scores (28 items) after rTMS treatment.

Microstructure changes in MDD-related brain connections:

An alternative hypothesis on the mechanism of antidepressant treatment is that rTMS can change generic MDD-related brain connections and treatment-response is associated with microstructure changes of specific connections even if they are not directly connected to the target. To this end, we investigated microstructure changes in seven white-matter fiber bundles between the four MDD-related brain regions, including the SGC, the dACC, the rACC, the CC, and two subregions of the left PFC, including the anterior-medial PFC (amPFC) and lateral PFC (lPFC). We also assessed if the dMRI changes were associated with the depression severity changes induced by TMS.

dMRI-based predictors for treatment response:

We further investigated if multidimensional dMRI measures of white-matter fiber bundles can predict the treatment response. To this end, we applied multivariate regression analysis to examine the correlation between the dMRI measures of each MDD-related brain connections or target-specific connections before treatment and the changes of HAMD scores. The analysis results can provide information to examine if the microstructure of specific white-matter connections can be used as predictors for treatment response for individual patients.

In summary, we have applied novel dMRI analysis to analyze data acquired from a unique cohort of subjects with MDD who underwent rTMS treatment with subject-specific targets. Our analysis results provide insights to understand if rTMS can change the microstructure of

white-matter connections related to stimulation target and to examine if treatment response is related to changes in white-matter microstructure and can be predicted by pre-treatment axonal microstructure.

2. Materials and Methods

2.1 Participants and study design

21 subjects (10 male and 11 female) were recruited from the Massachusetts General Hospital (MGH) TMS Clinical Service who met DSM-V criteria for major depressive disorder, recurrent, severe, without psychotic features. Determination of depression severity was first done with screening questionnaires, the Patient Health Quesionnaire-9 (PHQ9) [26] and the Quick Inventory of Depression Symptoms (QIDS SR-16) [27], and final determination of depression severity was determined upon evaluation by a psychiatrist. Subjects had failed at least four or more antidepressant medication trials or augmentation strategies from two or more antidepressant classes and had no contraindications to TMS (such as metallic implants in the head or neck area, implanted medical stimulators, cochlear implants), active substance use disorder, neurological abnormality, or history of seizure. Patients with history of schizophrenia, schizoaffective disorder, or bipolar affective disorder were excluded. All patients continued pre-TMS psychotropic medications during the TMS treatment course. Clinical assessments were collected at each clinical visit. MRI scans were obtained before the first rTMS treatment and after the entire treatment sessions. This study was approved by the Institutional Review Board of MGH. Informed consent was obtained from all subjects.

2.2 TMS treatment

rTMS was delivered using the MagVenture MagPro x100 (MagVenture, Farum, Denmark) equipped with B70 fluid cooled coil. Each patient received 36 sessions of rTMS using 10 Hz (4 second train duration and 11–26 second inter-train interval) to the left prefrontal cortex (PFC). Individualized prefrontal target selection was based on pre-treatment resting state functional connectivity, selecting the voxel in the left PFC with the strongest anticorrelation with the subgenual cingulate (see below for additional imaging methods details). Three-thousand pulses were delivered to left PFC targets at 120% of the resting motor threshold (MT). Each patient's resting MT was determined as the lowest percentage of the maximum stimulator output that provoked ≥50 μv motor evoked potentials in the contralateral first dorsal interosseus muscle in at least 50% of six trials when single pulses were delivered to the motor area. The first 30 treatments were applied 5 days per week (Monday-Friday) for 6 weeks and the last 6 treatments were tapered over the course of 2–3 weeks.

2.3 Clinical assessments

The Hamilton Depression Rating Scale (HAMD) [28] was used as a clinician-rated measure to capture depression severity on days 1 (before the first treatment), 10 (2 weeks), 20 (4 weeks), 30 (6 weeks) and 36 (end of treatment taper). The PHQ9 and QIDS scores were collected at the same times, and at the time of the clinical evaluation days prior to the first treatment.

2.4 MRI Data acquisition

MRI data were acquired from all subjects before the first rTMS treatment and after all treatment sessions. The imaging modalities included T1-weighted (T1w) MPRAGE, diffusion MRI (dMRI) and resting-state functional MRI (rs-fMRI). The dMRI scans were acquired at two b-values with b = 1000, 2000 s/mm^2, respectively, along 30 gradient directions on each b-shell, together with 4 b=0 s/mm^2 volumes. Other acquisition parameters of dMRI were as follows: data matrix size = 110×110×70, TE = 101ms, TR = 6500 ms, voxel size = 2×2×2 mm^3. The rs-fMRI data had the following parameters: data matrix size = 72×72×47, TE = 30 ms, TR = 3000 ms, voxel size = 3×3×3 mm^3, volume number = 124. The voxel size of the T1w image was 1×1×1 mm^3 and the data matrix size = 256×176×256.

2.5 Data preprocessing and analysis

2.5.1 $T1_w$ MRI preprocessing—T1w MRI data were processed using FreeSurfer [29] to obtain subject-specific brain label maps. The ANTs toolbox [30] was used to map the T1w image at the standard Montreal Neurological Institute (MNI) space to the subject-specific T1w images. The corresponding nonlinear registration transform was applied to map the Brodmann Area (BA) atlas in MNI space [31] to the T1w of patients in native space. FreeSurfer [29] label maps were used to obtain label maps for the dACC, rACC in the left hemisphere and the genu of CC. The BA atlas was used to identify the BAs 9, 10, 45 and 46. The combination of BAs 9 and 10 were considered as the anterior medial PFC (amPFC) and the combination of BAs 45 and 46 were considered as the lateral PFC (lPFC). In addition, we used the the manually drawn SGC seed region (which contains BA 25) as in [32] was used as the SGC.

2.5.2 rs-fMRI processing and rTMS targeting—Pre-rTMS rs-fMRI data was processed using the standard pipeline of SPM12 toolbox with the following steps: 1) dropping 4 initial volumes, 2) slice-time correction, 3) smoothing using a Gaussian kernel with 4-mm full width at half maximum (FHWM), 4) motion regression, 5) temporal filtering with passband between 0.01 and 0.08 Hz, 6) regression of nuisance signals from the WM and the CSF regions, 7) regression of global average signal. A manually drawn region in SGC gray matter as in [32] was used as the seed region in FC MRI. The voxel at the left PFC with the strongest anticorrelation with SGC was used as the stimulation target for rTMS treatment, as shown in Figure 2. Neuronavigation was used to place the TMS coil over the target coordinates.

2.5.3 dMRI processing and multi-fiber diffusion tractography—The dMRI data were first processed using a quality control toolbox, which is available at https://github.com/pnlbwh/SlicerDiffusionQC, to remove volumes with signal drops caused by motion. The remaining volumes were processed for motion corrections by applying linear registration to align the dMRI volumes to a baseline volume. Then, T1w MRI and dMRI baseline volume were co-registered using the ANTs toolbox [30] to correct for geometric distortions.

The multi-fiber tractography algorithm developed in [10] was applied to the processed dMRI data to compute the whole-brain tractography. The diffusion signal along the fiber bundles was modeled by two anisotropic components to characterize crossing fibers with

an additional isotropic-diffusion component to model free-water water in the extracellular space [6, 7]. The microstructural property of the tracts was characterized by several indices, including FW, FAt, RD, and AD. These measures provide more specific information than measures derived from the standard DTI approach [33] since the free-water-based method separately model isotropic fast-diffusion component in the extra axonal space and anisotropic slow-diffusion component in the axonal space.

2.5.4 Target-specific fiber bundles with E-field modeling—Our study cohort received individualized TMS therapy, using patient-specific cortical targets based on their unique pattern of functional connectivity. That said, when placing the coil over that target using neuronavigation, differences in head and brain anatomy can shape the actual topography and intensity of the induced electric fields on the cortex. To define white matter tracts around the region truly stimulated, we used E-field modeling based on the specific coil architecture and coil position (including 6 degrees of freedom), TMS parameters and individual anatomy from T1w scans to define the cortical target receiving the strongest electrical current. We used the SimNIBS pipeline [34] to simulate the E-field maps for each subject using individualized stimulation targets. Then, we followed the procedure in [35] to compute the location of the maximum electrical field intensity (i.e., E-max) which the average coordinate of 10 voxels in the gray matter with the strongest E-field magnitude. Then, we defined a 15-mm radius ball in the brain regions centered around the E-max as the subject-specific target region. The 15-mm radius was slightly larger than the focal range of E-field intensity, which is about 12 mm [36] to ensure that the underlying WM fiber bundles can be extracted in most subjects. Once the individual cortical stimulation target was defined, we applied the White Matter Query Language (WMQL) toolbox [37] and in-house written MATLAB programs, which is available at https://github.com/LipengNing/Utility, to extract the target-specific white-matter fiber bundles that connected the stimulation target regions to the SGC [3, 4, 14, 15], the dACC [17–20], the rACC [20–23], and the genu area of CC [24, 25].

2.5.5 MDD-related white-matter fiber bundles—For each subject, we also extracted 7 fiber bundles associated with the pathophysiology of MDD and connected to the left PFC region independent of target position. These fiber bundles were obtained by applying WMQL [37] to extract fiber bundles between the amPFC (BA 9 and BA 10), the lPFC (BA 45 and BA 46) and the four MDD-related deep-brain regions, i.e. SGC, the dACC, the rACC, and the genu area of CC. Then we used an in-house written MATLAB program to refine the fiber bundles to remove outliers. It should be noted that a connection between the lPFC and the SGC was not found in this dataset, which is consistent with results from studies on monkey brains which showed that isotope injected in BA 46 was not found in SGC, see Figure 6 in [38].

2.5.6 rTMS-related changes in clinical outcomes—To examine if rTMS improved clinical outcomes, we computed the changes of PHQ9 and QIDS scores from pre-rTMS to post-rTMS. For comparison, we also evaluated the changes of the two scores from the first clinical visit to the pre-rTMS visit and used them as a reference to examine if rTMS led

to more significant changes using paired t-test. Furthermore, we compared pre-rTMS and post-rTMS HAMD scores using paired t-tests.

2.5.7 Statistical analysis—Two analysis methods were applied to examine the changes of dMRI measures for each fiber bundle. First, we computed the mean FW, FAt, RD and AD measures for each of the extracted fiber bundles. Next, we applied paired t-test to examine if the dMRI measures of these target-specific tracts were altered by rTMS. In the second analysis, we tested the linear dependence between the changes of HAMD measures and the changes of dMRI measures in each extracted fiber bundle. The effects of age and gender on the changes of HAMD were adjusted using the generalized linear model (GLM). We performed a hypothesis test on the coefficients corresponding to the dMRI measures based on the F-statistic and examined the coefficient of determination, i.e., r^2, adjusted by the degree of freedom to analyze the accuracy of model fitting. Multiple testing correction was performed by controlling the False Discovery Rate (FDR) using the Benjamini-Hochberg (BH) procedure [39] across the four dMRI measures, including FW, FAt, RD, AD, in both analysis for each fiber bundle. Thus, 4 comparisons were performed for each fiber bundle. If the k-th lowest p value is lower or equal to $k/4\times0.05$, then all the null hypothesis corresponding to all the first k lowest p values are rejected.

To examine if multi-dimensional dMRI measures of specific fiber bundles before rTMS were related treatment response, we first implemented a feature selection procedure to select fiber bundles which had at least one pre-TMS dMRI measure that was correlated with the changes of HAMD scores with the significance level being $\alpha=0.05$. Then, we used multivariate regression analysis to analyze the linear dependence between the selected multi-dimensional dMRI measures and the changes of HAMD scores. The corresponding r^2 was adjusted according to the degree of freedom.

3. Results

3.1 On the changes of clinical measures

Figures 1(a) and 1(b) illustrate the changes PHQ9 and QIDS scores from the evaluation to pre-rTMS and the changes from pre-rTMS to post-rTMS. The two scores were stable before rTMS where the duration between evaluation and the first rTMS treatment was about 49 ± 29 days. rTMS led to more significant reductions in the two scores than the changes before rTMS treatment with the corresponding p-values being 0.003 and 0.031, respectively. Figure 1(c) shows that the post-TMS HAMD scores were also significantly lower than the pre-rTMS values ($p<1e-5$) (no HAMD scores were available on the day of the evaluation prior to treatment 1).

3.2 Microstructural changes in target-specific brain connections

Figure 2 illustrates the distribution of the rTMS targets of the 21 subjects mapped to a cortical surface in the MNI space (2a) as well as a representative patient example of the 4 treatment-specific tracts. Paired t-tests assessing the raw changes in diffusion properties after rTMS therapy showed no significant changes. The Target-SGC FW was reduced by treatment ($p=0.022$, see Figure S1 in the Supplementary Materials) but this was

not significant after correction for multiple comparisons (the corresponding significance threshold is 0.0125).

The correlation between changes in diffusion metrics and changes in clinical scores (HAMD-28) was also not significant.

3.3 Microstructural changes in MDD-related brain connections

Figure 3 illustrates the seven fiber bundles between the amPFC (yellow), the lPFC (magenta) and the four MDD-related brain regions. None of the three fiber bundles connected to the lPFC had significant changes in dMRI measures by rTMS treatment. Figure 4a shows that FW of SGC-amPFC fiber bundles was significantly increased (p*=0.006) by rTMS treatment. It should be noted that the RD of the SGC-amPFC was decreased by treatment (p=0.027, see Figure S1 in the Supplementary Materials) but that was not significant after correction for multiple comparisons (the corresponding threshold is 0.025).

Figure 4b to 4d illustrate rTMS increases in FAt (p*=0.002, Figure 4b) and AD (p*=0.004, Figure 4c), and reduced the RD (p*=0.007, Figure 4d) in the rACC-amPFC fiber bundles.

3.4 Correlation between changes in dMRI measures and HAMD

Figures 5(a) to 5(e) illustrates the correlation between the changes in the HAMD scores and changes in dMRI measures of the CC-lPFC, dACC-lPFC fiber bundles. In particular, Figure 5a shows that increased FAt values in the CC-lPFC fiber bundles were correlated with reduced HAMD scores (p*=0.013, r^2=0.375). Figure 5b shows that decreased RD values were correlated with improvement in the HAMD score (p*=0.017, r^2=0.358). Both correlations were significant after adjusting for multiple comparisons. Figures 5c and 5d show that increased FAt, AD and decreased RD of the dACC-lPFC fiber tracts were significantly correlated with decreased HAMD scores with p*=0.003, r^2=0.478, p*=0.034, r^2=0.308, p*=0.007, r^2=0.418, respectively. All three correlations were significant after adjusting for multiple comparisons with the FDR-controlling procedure.

3.5 Correlation between pre-rTMS dMRI measures and changes in HAMD

The pre-rTMS FAt, AD and RD measures of the dACC-lPFC fiber bundles were correlated with the changes of HAMD scores, with p=0.014, 0.047, 0,043, r^2=0.369, 0.285, 0.292, respectively, which are shown in Figure S2 in the Supplementary Materials. No other fiber bundles have shown correlation between the dMRI measures at the baseline and the changes of HAMD scores by rTMS. From multivariate regression analysis based on the identified dMRI measures, our analysis showed that the combination of the FAt, AD and RD scores could predict the changes of HAMD scores with (p*=0.01, r^2=0.505, see Fig. 5f), which was significant to reject a null hypothesis. Thus, the dMRI measures of the dACC-lPFC fiber bundles can potentially provide predictors for treatment response for individual patients.

4. Discussion

In this work, we have analyzed the MRI data and clinical measures collected from 21 patients with MDD who were treatment-resistant to standard medication therapy and

underwent rTMS treatment. This is a unique database where all subjects were treated using subject-specific stimulation targets in the DLPFC determined by FC to the SGC. Our analysis integrates novel free-water based dMRI measures from several MDD-related and target-related fiber bundles to examine rTMS-related microstructural changes, response biomarkers and predictors for treatment response. The main results are summarized and discussed below.

Our results show that a course of rTMS antidepressant treatment in patients with MDD did not affect the white matter properties of tracts emerging directly from the individual TMS targets (defined based on functional connectivity MRI and E-field modeling) nor the more generic depression-related tracts from the lateral PFC (where TMS was applied) and deeper limbic nodes. Nonetheless, we observed that rTMS significantly altered the microstructure of anterior-medial PFC fiber bundles, including increased FW in the SGC-amPFC fibers and increased FAt and AD, and reduced RD in the rACC-amPFC fibers. These findings highlight and confirm the circuit-level mechanisms of action of TMS, by failing to identify changes in the areas directly stimulated by TMS but revealing changes in distal disease-relevant structures. Again, the TMS targets appear to function as windows that provide access to modulate circuit of interest broadly but may be directly unaffected by the intervention while plastic changes take place distally in the network. The amPFC WM may have relative higher plasticity so that the underlying tissue microstructure is particularly sensitive to rTMS, even when applied in distal but connected cortical nodes. dMRI measures, such as the conventional FA, have been applied in previous studies investigate rTMS related changes in tissue microstructure [40, 41]. But the conventional FA measure does not provide specific measure of tissue microstructure. For example, an increased FA measure can be related to improvements in myelin sheath, reduction in axonal undulations or reduction in extra-cellular space [42–44]. The free-water based dMRI measures can separately characterize the microstructure of intra-cellular and extra-cellar space, thus improve the specificity of dMRI measures. The increased FW measures indicated that rTMS may have increased extra-cellualr space of the SGC-amPFC fiber bundles. On the other hand, the rACC-amPFC tracts did not have significant changes in the extra-cellular space. The reduced RD and increased AD measures in the intra-celluar space led to the increased FAt, which may be related to reduced undulations of axonal fiber bundles [44], i.e. the fiber bundles were less curved at the microscopic scale to enhance the connectivity between brain regions especially for patients with treatment-resistant depression.

While the strongest raw changes in white matter properties were described in antero-medial PFC fibers, these changes did not correlate with clinical response. Nevertheless, the weaker (and not significant) raw changes in lateral PFC tracts diffusion properties were significantly correlated with the therapeutic response (i.e., reduction in HAMD28 scores). This finding is compelling, and it reveals an interesting phenomenon in which stronger raw changes associated with the intervention fail to show a true relationship with the clinical effects, while weaker non-significant (though showing a trend) effects are more clinically meaningful by explaining the variability in the clinical response and hence acting as a response biomarkers or treatment target. It is also interesting that the association between diffusion changes and the clinical response does happen in tracts emerging from the lateral PFC that we stimulate directly. The tracts derived from the patient-specific stimulation

targets though failed to show either raw changes in diffusion properties or an association between these biological changes and the clinical response. The smaller size of the cortical seeds and the fiber bundles themselves may be a technical reason to explain the absence of findings in the precise and individualized targets of interest, but biological reasons such as the ones exposed in the above paragraph could also explain this result.

Our analysis shows that reduced HAMD scores are correlated with increased FAt and decreased RD measures of the CC-lPFC fiber bundles and are also correlated with increased FAt, AD and decreased RD of the dACC-lPFC fiber bundles. Similar to target-related bundles, increased AD and decreased RD may be related to improved structural connectivity, i.e. the fiber bundles are less undulated and more straight to enhance the connectivity between brain regions [44]. But the microstructural measures of the two fiber bundles are not statistical different between pre-treatment and post-treatment measures, which indicate that the underlying tissue may have relative lower overall plasticity compared with amPFC white matter (though it is more clinically relevant). Moreover, the microstructural changes of lPFC WM are more effective to improves clinical outcomes, which is consistent to the standard brain targeting position at the DLPFC [4].

Brain functional connectivity or activity measured by resting state functional MRI [45–47], electroencephalography (EEG) [48, 49] or single photon emission computed tomographay (SPECT) [50] have been shown to provide predictors for rTMS treatment response for MDD. Our analysis has provided complementary information that dMRI measures of brain structural connections can be useful predictors for treatment response. Lower FAt, AD and higher RD of the dACC-lPFC fiber bundles before rTMS were correlated with better treatment response, as shown in Figure 9. This indicates that rTMS may have better potential to improve the underlying structural connections if they are more undulated or altered at the baseline.

This study has several limitations. First and foremost, the statistical power of the analysis is limited by the relatively small number of subjects. Future and ongoing studies with larger samples acquiring dMRI measures before, during and after rTMS treatment should provide greater certainty on the effects of rTMS on white matter properties, and their clinical significance. Moreover, we did not include control or sham subjects with imaging measures to contextualize the rTMS-related microstructural changes, although this is partly compensated using correlational analyses and within-subject anatomical controls.

5. Conclusion

We summarize that this study has shown that dMRI together with novel analysis methods can provide a useful tool identify treatment targets (i.e., response biomarkers) and predictors of response for rTMS in patients with MDD.

Supplementary Material

Refer to Web version on PubMed Central for supplementary material.

Role of the funding source

The authors declare no conflict of interest. The authors would like to acknowledge the following grants which supported this work: NIH grant R21MH115280 to LN and JAC, R01MH112737 to JAC, R21MH126396, R21MH116352 and K01MH117346 to LN.

Reference

1. George MS, et al. , Daily left prefrontal transcranial magnetic stimulation therapy for major depressive disorder: a sham-controlled randomized trial. Arch Gen Psychiatry, 2010. 67(5): p. 507–16. [PubMed: 20439832]
2. O'Reardon JP, et al. , Efficacy and safety of transcranial magnetic stimulation in the acute treatment of major depression: a multisite randomized controlled trial. Biol Psychiatry, 2007. 62(11): p. 1208–16. [PubMed: 17573044]
3. Fox MD, et al. , Efficacy of transcranial magnetic stimulation targets for depression is related to intrinsic functional connectivity with the subgenual cingulate. Biol Psychiatry, 2012. 72(7): p. 595–603. [PubMed: 22658708]
4. Fox MD, Liu H, and Pascual-Leone A, Identification of reproducible individualized targets for treatment of depression with TMS based on intrinsic connectivity. Neuroimage, 2013. 66: p. 151–60. [PubMed: 23142067]
5. Thielscher A, Antunes A, and Saturnino GB, Field modeling for transcranial magnetic stimulation: A useful tool to understand the physiological effects of TMS? Annu Int Conf IEEE Eng Med Biol Soc, 2015. 2015: p. 222–5. [PubMed: 26736240]
6. Pasternak O, Kubicki M, and Shenton ME, In vivo imaging of neuroinflammation in schizophrenia. Schizophr Res, 2016. 173(3): p. 200–212. [PubMed: 26048294]
7. Pasternak O, et al. , Free water elimination and mapping from diffusion MRI. Magn Reson Med, 2009. 62(3): p. 717–30. [PubMed: 19623619]
8. Pasternak O, et al. , The extent of diffusion MRI markers of neuroinflammation and white matter deterioration in chronic schizophrenia. Schizophr Res, 2015. 161(1): p. 113–8. [PubMed: 25126717]
9. Baumgartner C, et al. Filtered multi-tensor tractography using free water estimation. In International Society for Magnetic Resonance in Medicine Meeting 2012.
10. Malcolm JG, Shenton ME, and Rathi Y, Filtered multitensor tractography. IEEE Trans Med Imaging, 2010. 29(9): p. 1664–75. [PubMed: 20805043]
11. Reddy CP and Rathi Y, Joint Multi-Fiber NODDI Parameter Estimation and Tractography Using the Unscented Information Filter. Front Neurosci, 2016. 10: p. 166. [PubMed: 27147956]
12. Tang Y, et al. , Altered Cellular White Matter But Not Extracellular Free Water on Diffusion MRI in Individuals at Clinical High Risk for Psychosis. Am J Psychiatry, 2019. 176(10): p. 820–828. [PubMed: 31230461]
13. Pasternak O, et al. , Excessive extracellular volume reveals a neurodegenerative pattern in schizophrenia onset. J Neurosci, 2012. 32(48): p. 17365–72. [PubMed: 23197727]
14. Drevets WC, Savitz J, and Trimble M, The subgenual anterior cingulate cortex in mood disorders. CNS Spectr, 2008. 13(8): p. 663–81. [PubMed: 18704022]
15. Mayberg HS, Defining the neural circuitry of depression: toward a new nosology with therapeutic implications. Biol Psychiatry, 2007. 61(6): p. 729–30. [PubMed: 17338903]
16. Mayberg HS, et al. , Deep brain stimulation for treatment-resistant depression. Neuron, 2005. 45(5): p. 651–60. [PubMed: 15748841]
17. Goodkind M, et al. , Identification of a common neurobiological substrate for mental illness. JAMA Psychiatry, 2015. 72(4): p. 305–15. [PubMed: 25651064]
18. Reynolds S, et al. , Cortical thickness in youth with major depressive disorder. BMC Psychiatry, 2014. 14: p. 83. [PubMed: 24645731]
19. Smoski MJ, et al. , fMRI of alterations in reward selection, anticipation, and feedback in major depressive disorder. J Affect Disord, 2009. 118(1–3): p. 69–78. [PubMed: 19261334]

20. Zhao Y, et al. , Gray Matter Abnormalities in Non-comorbid Medication-naive Patients with Major Depressive Disorder or Social Anxiety Disorder. EBioMedicine, 2017. 21: p. 228–235. [PubMed: 28633986]
21. Gunning FM, et al. , Anterior cingulate cortical volumes and treatment remission of geriatric depression. Int J Geriatr Psychiatry, 2009. 24(8): p. 829–36. [PubMed: 19551696]
22. Pizzagalli D, et al. , Anterior cingulate activity as a predictor of degree of treatment response in major depression: evidence from brain electrical tomography analysis. Am J Psychiatry, 2001. 158(3): p. 405–15. [PubMed: 11229981]
23. Yoshimura S, et al. , Rostral anterior cingulate cortex activity mediates the relationship between the depressive symptoms and the medial prefrontal cortex activity. J Affect Disord, 2010. 122(1–2): p. 76–85. [PubMed: 19589603]
24. Dillon DG, et al. , Depression is associated with dimensional and categorical effects on white matter pathways. Depress Anxiety, 2018. 35(5): p. 440–447. [PubMed: 29486093]
25. Jiang J, et al. , Microstructural brain abnormalities in medication-free patients with major depressive disorder: a systematic review and meta-analysis of diffusion tensor imaging. J Psychiatry Neurosci, 2017. 42(3): p. 150–163. [PubMed: 27780031]
26. Kroenke K, PHQ-9: global uptake of a depression scale. World Psychiatry, 2021. 20(1): p. 135–136. [PubMed: 33432739]
27. Brown ES, et al. , The Quick Inventory of Depressive Symptomatology-Self-report: a psychometric evaluation in patients with asthma and major depressive disorder. Ann Allergy Asthma Immunol, 2008. 100(5): p. 433–8. [PubMed: 18517074]
28. Hamilton M, A rating scale for depression. J Neurol Neurosurg Psychiatry, 1960. 23: p. 56–62. [PubMed: 14399272]
29. Fischl B, FreeSurfer. Neuroimage, 2012. 62(2): p. 774–81. [PubMed: 22248573]
30. Avants BB, et al. , A reproducible evaluation of ANTs similarity metric performance in brain image registration. Neuroimage, 2011. 54(3): p. 2033–44. [PubMed: 20851191]
31. Lacadie CM, et al. , More accurate Talairach coordinates for neuroimaging using non-linear registration. Neuroimage, 2008. 42(2): p. 717–25. [PubMed: 18572418]
32. Ning L, et al. , Limits and reproducibility of resting-state functional MRI definition of DLPFC targets for neuromodulation. Brain Stimul, 2019. 12(1): p. 129–138. [PubMed: 30344110]
33. Basser PJ, Mattiello J, and LeBihan D, Estimation of the effective self-diffusion tensor from the NMR spin echo. J Magn Reson B, 1994. 103(3): p. 247–54. [PubMed: 8019776]
34. Windhoff M, Opitz A, and Thielscher A, Electric field calculations in brain stimulation based on finite elements: an optimized processing pipeline for the generation and usage of accurate individual head models. Hum Brain Mapp, 2013. 34(4): p. 923–35. [PubMed: 22109746]
35. Lee EG, et al. , Impact of non-brain anatomy and coil orientation on inter- and intra-subject variability in TMS at midline. Clin Neurophysiol, 2018. 129(9): p. 1873–1883. [PubMed: 30005214]
36. Thielscher A and Kammer T, Electric field properties of two commercial figure-8 coils in TMS: calculation of focality and efficiency. Clin Neurophysiol, 2004. 115(7): p. 1697–708. [PubMed: 15203072]
37. Wassermann D, et al. , The white matter query language: a novel approach for describing human white matter anatomy. Brain Struct Funct, 2016. 221(9): p. 4705–4721. [PubMed: 26754839]
38. Barbas H and Pandya DN, Architecture and intrinsic connections of the prefrontal cortex in the rhesus monkey. J Comp Neurol, 1989. 286(3): p. 353–75. [PubMed: 2768563]
39. Benjamini Y, et al. , Controlling the false discovery rate in behavior genetics research. Behav Brain Res, 2001. 125(1–2): p. 279–84. [PubMed: 11682119]
40. Abe M, Fukuyama H, and Mima T, Water diffusion reveals networks that modulate multiregional morphological plasticity after repetitive brain stimulation. Proc Natl Acad Sci U S A, 2014. 111(12): p. 4608–13. [PubMed: 24619090]
41. Kozel FA, et al. , Fractional anisotropy changes after several weeks of daily left high- frequency repetitive transcranial magnetic stimulation of the prefrontal cortex to treat major depression. J ECT, 2011. 27(1): p. 5–10. [PubMed: 20559144]

42. Zhang H, et al. , NODDI: practical in vivo neurite orientation dispersion and density imaging of the human brain. Neuroimage, 2012. 61(4): p. 1000–16. [PubMed: 22484410]

43. O'Donnell LJ and Pasternak O, Does diffusion MRI tell us anything about the white matter? An overview of methods and pitfalls. Schizophr Res, 2015. 161(1): p. 133–41. [PubMed: 25278106]

44. Nilsson M, et al. , The importance of axonal undulation in diffusion MR measurements: a Monte Carlo simulation study. NMR Biomed, 2012. 25(5): p. 795–805. [PubMed: 22020832]

45. Avissar M, et al. , Functional connectivity of the left DLPFC to striatum predicts treatment response of depression to TMS. Brain Stimul, 2017. 10(5): p. 919–925. [PubMed: 28747260]

46. Dichter GS, Gibbs D, and Smoski MJ, A systematic review of relations between resting-state functional-MRI and treatment response in major depressive disorder. J Affect Disord, 2015. 172: p. 8–17. [PubMed: 25451389]

47. Philip NS, et al. , Network Mechanisms of Clinical Response to Transcranial Magnetic Stimulation in Posttraumatic Stress Disorder and Major Depressive Disorder. Biol Psychiatry, 2018. 83(3): p. 263–272. [PubMed: 28886760]

48. Zandvakili A, et al. , Use of machine learning in predicting clinical response to transcranial magnetic stimulation in comorbid posttraumatic stress disorder and major depression: A resting state electroencephalography study. J Affect Disord, 2019. 252: p. 47–54. [PubMed: 30978624]

49. Hasanzadeh F, Mohebbi M, and Rostami R, Prediction of rTMS treatment response in major depressive disorder using machine learning techniques and nonlinear features of EEG signal. J Affect Disord, 2019. 256: p. 132–142. [PubMed: 31176185]

50. Langguth B, et al. , Pre-treatment anterior cingulate activity as a predictor of antidepressant response to repetitive transcranial magnetic stimulation (rTMS). Neuro Endocrinol Lett, 2007. 28(5): p. 633–8. [PubMed: 17984932]

Highlights:

- rTMS-induced microstructural changes in patients with depression are examined using dMRI
- Subject-specific brain targets were used for treatment based on the functional connectivity
- rTMS has changed dMRI measures in fiber bundles connected the anterior-medial-prefrontal cortex
- Changes in dMRI measures of lateral-prefrontal fiber bundles are related with improved response
- dMRI measures of lateral-prefrontal fiber bundles at baseline can predict treatment response

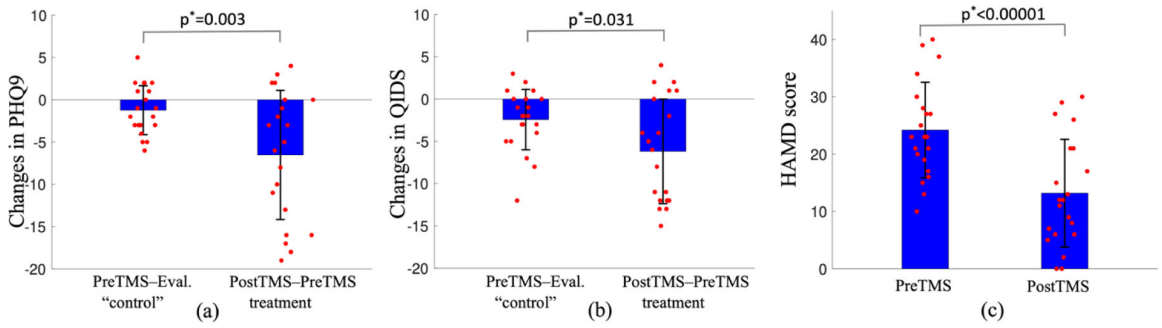

Figure 1:

Comparison of rTMS-related changes of clinical measures. Figures (a) and (b) show that rTMS-related reductions in PHQ9 and QIDS scores are significantly larger than the changes between Pre-rTMS and the evaluation in 49 ± 29 days using paired one-sided t-test, indicating rTMS is effective on this group of subjects. Figure (c) shows that the postTMS HAMD scores are significantly lower than PreTMS scores.

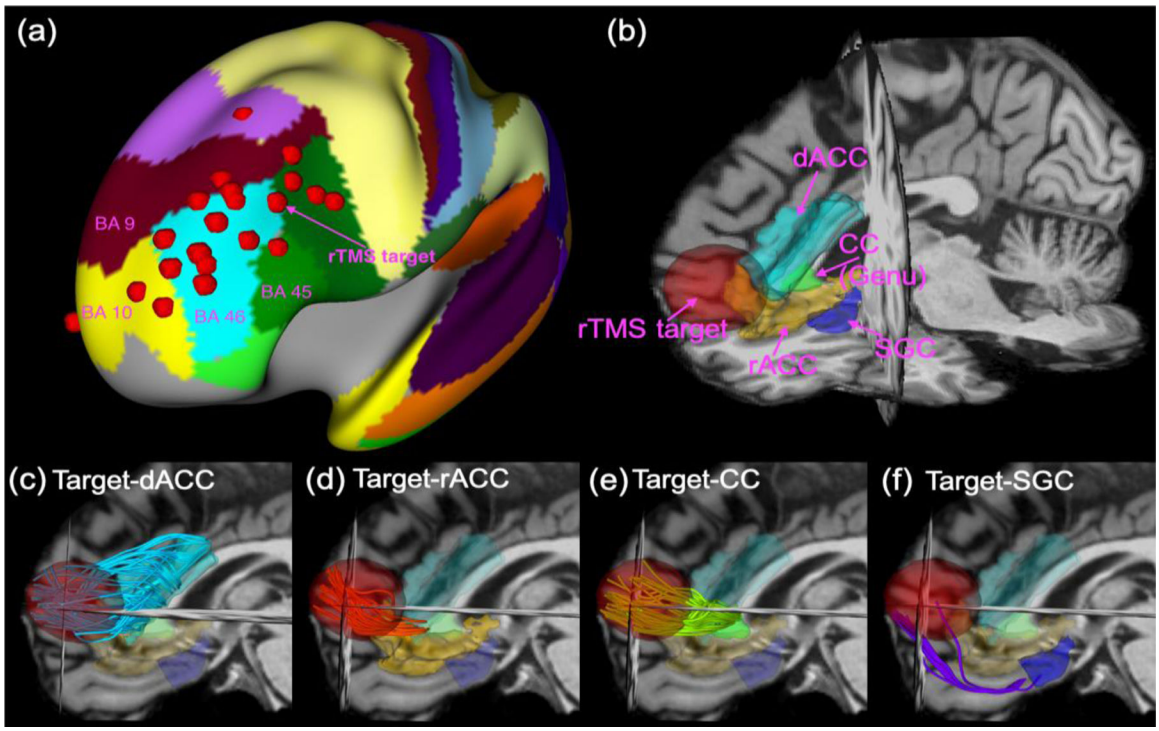

Figure 2:

The red dots in (a) illustrate the stimulation targets of 21 subjects mapped on the cortical surface in the MNI space with the background being the label maps for the Brodmann areas. Fig. (b) illustrates the target region, i.e. 15-mm-radius ball around the maximum of E-field intensity, and four MDD-related deep-brain regions, including the dACC, rACC, CC and SGC for one representative subject. Figs. (c)-(f) illustrate the fiber bundles from diffusion-MRI tractography that connect the stimulation target to the dACC, the rACC, the genu of CC and the SGC, respectively.

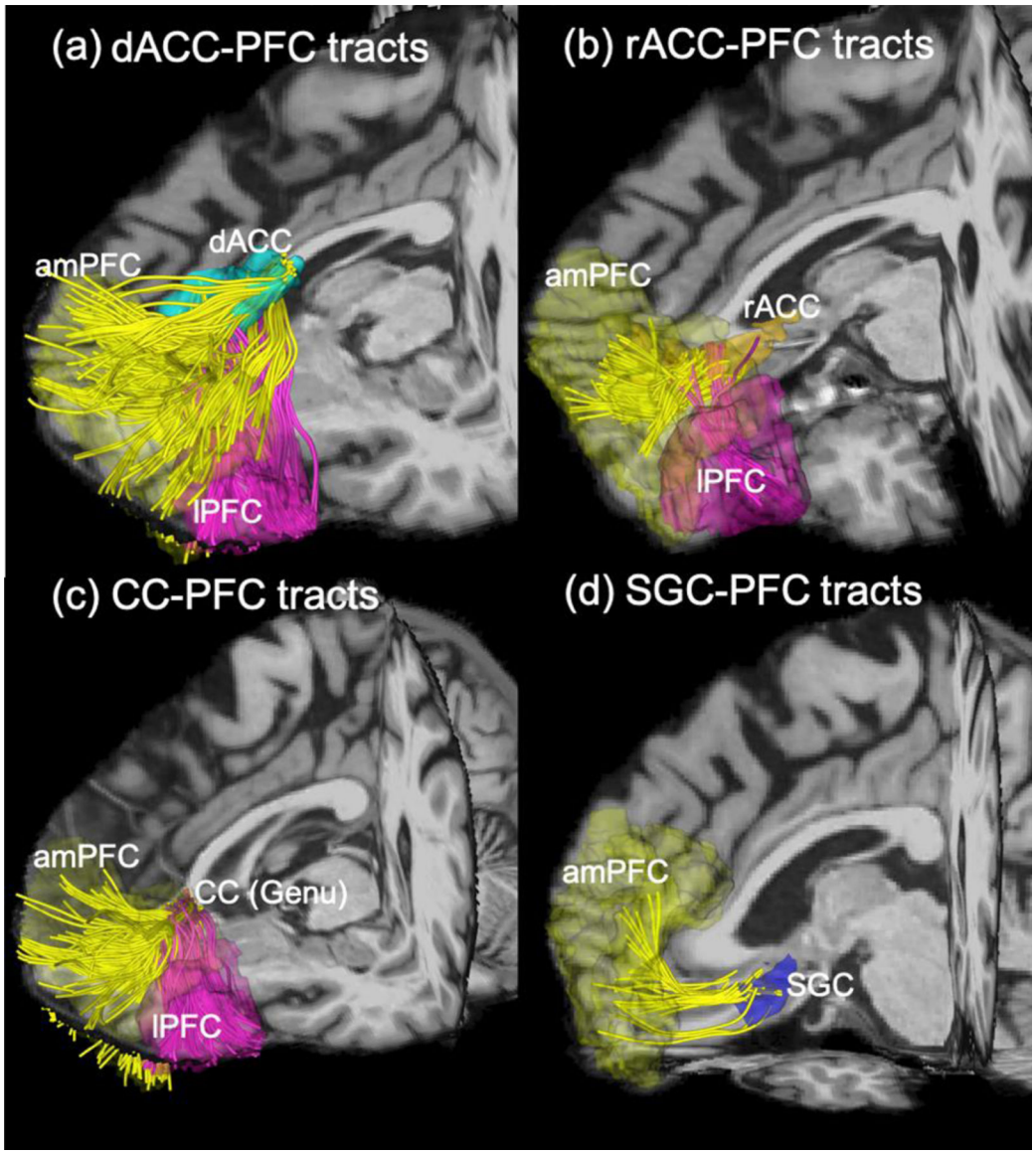

Figure 3:

Diffusion-MRI tractography showing fiber bundles connected to different subregions of the left PFC and four MDD-related deep-brain regions: (a)-(c) illustrate the fiber bundles that connect the amPFC (yellow), lPFC (magenta) and the dACC, the rACC, and the genu of CC, respectively, and (d) illustrate the fiber bundles between the amPFC and the SGC. There is no connection between lPFC and SGC.

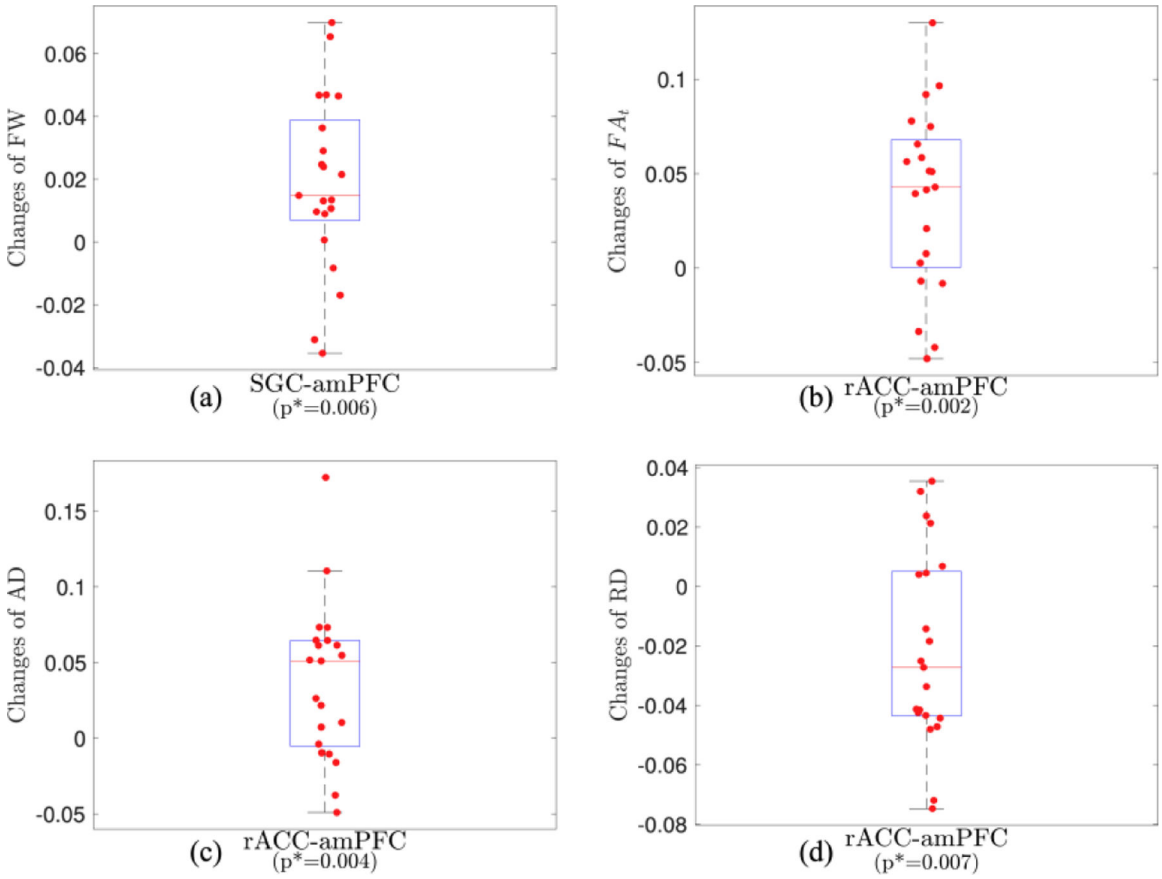

Figure 4:

Changes of dMRI measures of SGC-amPFC (a) and rACC-amPFC (b,c,d) fiber bundles by rTMS treatment.

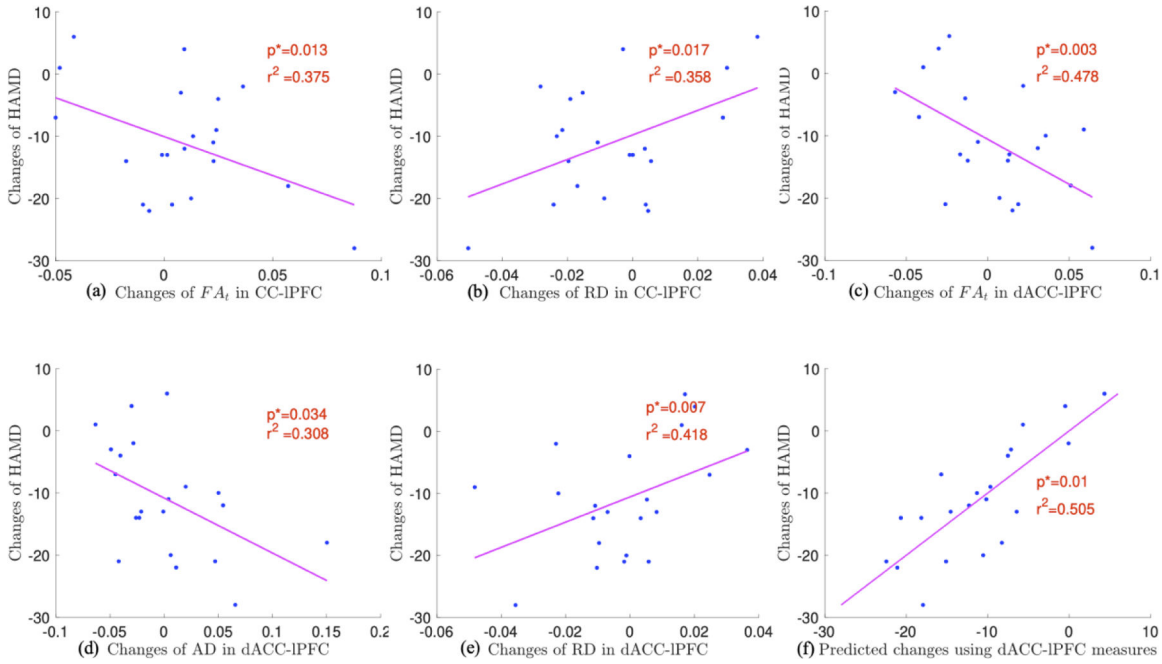

Figure 5:

Correlations between the changes of HAMD scores and the changes of dMRI measures of CC-lPFC (a,b), the dACC-lPFC (c,d,e) fiber bundles and pre-TMS FAt, RD, AD measures of dACC-lPFC (f).